Heliyon 10 (2024) e24214

Contents lists available at ScienceDirect

Heliyon

journal homepage: www.cell.com/heliyon

Research article

Exploration of anode candidacy of $Ni_{0.2}Co_{2.8}O_4$ and integrated $Ni_{0.2}Co_{2.8}O_4$/MWCNTs in supercapacitor and oxygen evolution reaction

Sana Sabahat [a,**], Nasima Arshad [b,*], Nida Aftab [a], Zeeshan Mujtaba [b], Mohd Afzal [c], Maria Christy [d]

[a] Department of Chemistry, COMSATS University, Islamabad, 44000, Pakistan
[b] Department of Chemistry, Allama Iqbal Open University, Islamabad, 44000, Pakistan
[c] Department of Chemistry, College of Science, King Saud University, Riyadh, 11451, Saudi Arabia
[d] Department of Energy Engineering, Hanyang University, 222 Wangsimni-ro, Seongdong-gu, Seoul, 04763, South Korea

ARTICLE INFO

Keywords:
$Ni_{0.2}Co_{2.8}O_4$/MWCNTs
Facile synthesis
Anode candidate
Electrochemical performance
Supercapacitor & OER applications

ABSTRACT

In the current research work, $Ni_{0.2}Co_{2.8}O_4$ and $Ni_{0.2}Co_{2.8}$/MWCNTs have been synthesized via facile sol-gel and wet impregnation method. The synthesized materials attained the crystalline structures as evident from X-ray diffraction analysis (XRD). The uniform morphology and well dispersion of $Ni_{0.2}Co_{2.8}O_4$ onto MWCNTs was observed via scanning electron microscopy (SEM). The electrochemical investigations for supercapacitor application by cyclic voltammetry (CV), galvanostatic charge discharge (GCD), and electrochemical impedance spectroscopy (EIS) revealed that, among both materials, $Ni_{0.2}Co_{2.8}O_4$/MWCNTs has high specific capacitance (CV; 505.8 Fg^{-1} at 5 mV/s, GCD; 1598 Fg^{-1} at 0.5 A/g), greater capacitance retention (85 %) at 1000 cycles and has lower charge transfer resistance (R_{ct}; 3.48 Ω cm^2). These findings reflected the potential candidacy of $Ni_{0.2}Co_{2.8}O_4$/MWCNTs to be used as anode material in supercapacitor. Further investigations by CV and linear sweep voltammetry (LSV) for oxygen evolution reaction (OER) activity in 1.0 M KOH showed comparatively low over potential of 340 mV @100 mA/cm^2 for the same integrated material. Additionally, the lower Tafel slope (47 mV/dec) and solution resistance authenticated it as an appropriate electrocatalyst for OER in water splitting. The CPE (controlled potential electrolysis) revealed the stability of both materials for OER in water oxidation.

1. Introduction

Non-renewable energy sources i.e., coal, natural gas, oil, and nuclear reactors are not only dangerous to our environment and health but about to expire due to their extensive usage. All over the world, the economic system is shifting to utilize renewable energy sources that mainly includes solar, wind, marine, biowaste, water, geothermal, biogas sources etc. [1]. The popularity and demand of renewable energy sources, often-called sustainable sources, increases day by day as these sources are harmless to the environment and

* Corresponding author.
** Corresponding author.
E-mail addresses: s.sabahat@comsats.edu.pk (S. Sabahat), nasimaa2006@yahoo.com (N. Arshad).

https://doi.org/10.1016/j.heliyon.2024.e24214
Received 6 September 2023; Received in revised form 3 January 2024; Accepted 4 January 2024
Available online 9 January 2024

available at no cost. Therefore, the tuning of renewable energy sources is one of the ways to climate change.

In the recent scenario, a prodigious development in new energy storage systems is needed that should have efficient performance not only in term of high-power density, stability but also recognize for cost effectiveness [2–5]. Supercapacitors are considered as potential candidates due to their long-term stability, high life cycle and efficient charging-discharging system [6,7]. Typically, pseudo-capacitors have larger specific capacitance and higher energy density but low cycling life than electric double layer capacitors (EDLCs) that have excellent performance, but low energy potential and charge only confined to the surface [8]. Interestingly, EDLCs and pseudo capacitors separately contributed towards the total electrochemical and capacitance value of a supercapacitor. However, EDLCs and pseudo capacitors in combination is the more tempting approach to describe the supercapacitor performance of electrochemically addressable materials like mixed transition metal oxides (MTMO). In this way a correct description of these capacitors could be studied under a single term which is known as hybrid capacitors.

In recent years, spinal structures transition metal oxides $A_xB_{3-x}O_4$ (where A and B are two different transition metals) have gained much attraction for their electrode candidacy in energy storage applications. Ni, Co, and its co-materials contain enhanced electrochemical performances as electrode materials, therefore has remarkable contribution as energy materials [9–13]. Among various spinel metal cobaltites, the nickel cobaltite ($NiCo_2O_4$) has been reported to have extensive applications in catalysis [14]. Besides the low cost and less toxicity, the fast oxidation reduction reaction in nickel cobaltite is favored due to multi-oxidation states that result in excellent sp. Capacitance [14]. In comparison to individual nickel oxide (NiO) or cobalt oxide (Co_3O_4), the nickel cobaltite ($NiCo_2O_4$) has been found to be promising for supercapacitors with greater electrical and electrochemical performances [15]. Moreover, in comparison to binary metal oxides, the mesoporous structure of nickel cobaltite provides more electroactive sites for the interaction between electrode and electrolyte and hence improves the capacitive performance [14–16].

In 1991, MWCNTs (multi-walled carbon nanotubes) were first time discovered by Iijiama [17]. Due to their thermal and electrical stability, porous and hollow structure makes them an important nanomaterial for various applications [18–23]. Literature on the insertion of mixed transition metal oxides onto carbonaceous sp^2 materials like CNTs is rare and reported that the properties of MWCNTs can be improved via this fabrication [24]. The insertion of MTMO results in enhancing electrons' kinetics and the diffusion of ions at the interface (electrode – electrolyte). The introduction of MWCNTs provides superior thermal conductivity, good structural tenacity, and excellent electrochemical performance of energy storage devices [25–30]. CNTs (up to1300 m^2/g) possess a high exohedral surface area due to which interaction between electrode and electrolyte during a redox activity would be greater.

Considering the impact of MWCNTs and nickel cobaltite on capacitive performance, the current study is focused to integrate $Ni_{0.2}Co_{2.8}O_4$ with MWCNTs. Both supported and unsupported synthesized materials ($Ni_{0.2}Co_{2.8}O_4$/MWCNTs and $Ni_{0.2}Co_{2.8}O_4$) were further investigated for their electrochemical performance as anode candidates in supercapacitor and OER applications.

2. Experimental

2.1. Materials

High grade chemicals and reagents were used in current studies including nickel nitrate $Ni(NO_3)_2.6H_2O$, cobalt nitrate $Co(NO_3)_2.6H_2O$, (Uni-chem Ltd), anhydrous citric acid (Sigma-Aldrich), ethylene glycol (Sigma-Aldrich), multi-walled carbon nanotubes (main range of diameter; < 2 nm), 2×2 cm^2 chip of nickel foam, nafion solution (5 %), potassium hydroxide (Sigma-Aldrich) and deionized water.

2.2. XRD and SEM analyses

The synthesized materials were analyzed for their structures and morphology. The structural measurements were carried out using Cu-KαX-ray diffraction (1.5418 Å) with the diffraction angle of 10°–70° and the crystallite size of the sample was determined from XRD pattern using Scherer's equation. The morphology of prepared material was studied using FEI Nova 450 Nano SEM.

2.3. Materials' synthesis

The sol-gel synthetic protocol was used to synthesize $Ni_{0.2}Co_{2.8}O_4$. The stoichiometric amount of nitrate precursors of nickel and cobalt; $Co(NO_3)_2.6H_2O$ (15.9 g), $Ni(NO_3)_2.6H_2O$ (1.163 g) was used. Anhydrous citric acid (15.37 g) was added as a chelating agent. Briefly, in homogenous solutions of precursors, citric acid was added slowly. The temperature was raised to 80 °C along with continuous stirring. The temperature was raised to 80 °C along with continuous stirring. After 2 h the temperature was raised to 110 °C till the gelation occurred followed by drying in electric oven for 9 h. The sample was further calcined at 900 °C for 8 h. The dark blackish dried sample was grinded and characterized.

For the functionalization of MWCNTs, H_2SO_4 and HNO_3 were used in a 1:3 ratio in which 100 mg MWCNTs were soaked and then ultrasonicated for 6 h [31]. Washing of the subsequent mixture was done several times with distilled water till the filtrate attained neutral pH. The functionalized MWCNTs were oven dried for 12 h by keeping the temperature at 100 °C.

For synthesis of supported electrocatalyst ($Ni_{0.2}Co_{2.8}O_4$/MWCNTs), wet impregnation method was employed [31–34]. The weight percent loading of MWCNTs to $Ni_{0.2}Co_{2.8}O_4$ was done. Briefly, in a stoichiometric amount (same as used for unsupported sample) of nickel and cobalt nitrate solutions, 10 mL of $C_2H_6O_2$ (ethylene glycol) was added which acts as a reducing agent. Lastly, weighed (0.061 g) functionalized MWCNTs were added in the solution followed by ultrasonication for 30 min at 0 °C. The temperature was maintained at 100 °C for 3 h and was stirred at 450 rpm. To attain the sample morphology, it was calcined first for 2 h at 450 °C and

then kept for 6 h in vacuum oven at 200 °C. A black color sample was obtained that was dried and then finally grinded to fine powder to avoid any granules or fragments. The synthetic protocols are provided in Scheme 1.

2.4. Electrochemical cell setup and electrode fabrication

Electrochemical studies were carried out on GAMRY-3000 potentiostat/galvanostat/ZRA (USA). The electrochemical measurements were made within a three-electrode cell system. Modified Ni-foam with MWCNTs supported and unsupported structures were used as the working electrodes; platinum (Pt) wire and Ag/AgCl were the counter and reference electrodes, respectively. In the three-electrode system, a 2 × 2 cm^2 chip of nickel foam was used to fabricate the synthesized material on it to be used as working electrode. The fabrication was done by, initially, sonicating the synthesized material for 10–15 min 0.5 mL nafion solution (5 %) was then added as a binder to the sonicated material and then firmly applied to nickel foam. The prepared electrode was dried by keeping it in an oven (85 °C) for 15 h. The aqueous potassium hydroxide (1 mol/dm^3) solution was used as electrolyte.

2.5. Electrochemical procedures

The CV and GCD (chronopotentiometry) measurements were carried out at room temperature at different scan rates and at different current densities keeping the potential window between 0 and 0.7 V vs. Ag/AgCl electrode. The Nyquist plots were drawn through EIS at open circuit potential and the frequency range was selected 100 kHz–10 mHz (amplitude of AC sine waves = 5 mV). The stability of investigated materials for supercapacitor application was monitored by CV cycling.

For water oxidation activity, the scanning for OER was performed at 5 mV/s by CV and LSV in 1.0 M KOH solution. Before running these experiments, the conversion of potential was made to potential of reverse hydrogen electrode (E_{RHE}) using Nernst equation {$E_{RHE} = E_{Ag/AgCl} + 0.059\ pH + E^{o}_{Ag/AgCl}$} [35]. The voltammograms were scanned with uncompensated and compensated IR-drop. The voltammograms with uncompensated IR-drop included the resistance due to electrolyte present in the solution whereas with compensated IR-drop the resistance due to 1.0 M KOH electrolyte was excluded. For overpotential calculation, the Tafel plots were drawn as overpotential (V) vs. log j (A/cm^2) by using the equations {($\eta = E_{RHE}$ - 1.23 V); ($\eta = +\ b \log j + a$)} and the Tafel slope (b) was evaluated. The electrode material's stability for OER in water splitting was monitored by chronoamperometry (controlled potential electrolysis; CPE), while keeping the potential of the electrode constant at 1.65 V vs. RHE.

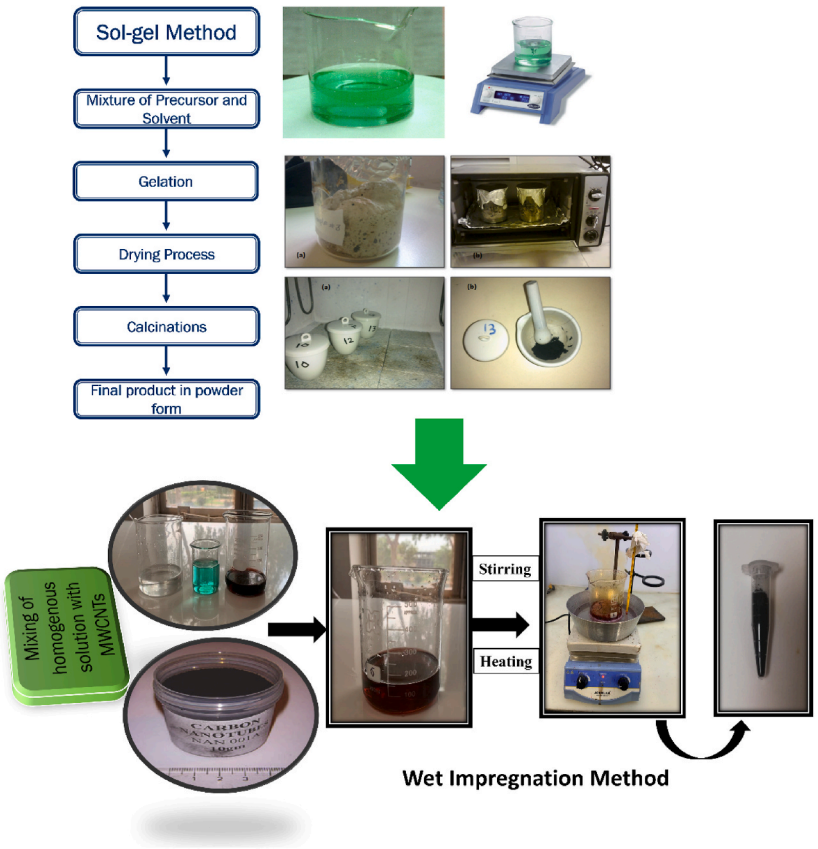

Scheme 1. Synthetic protocols for $Ni_{0.2}Co_{2.8}O_4$ and $Ni_{0.2}Co_{2.8}O_4$/MWCNTs.

3. Results and discussion

3.1. X-ray diffraction studies (XRD)

Fig. 1 shows the stacked XRD patterns of $Ni_{0.2}Co_{2.8}O_4$ and $Ni_{0.2}Co_{2.8}O_4$/MWCNTs. All the peaks are indexed based on the cubic spinel crystal structure of $NiCo_2O_4$ (JCPDS card # 20–0781). Both the synthesized samples have attained a high degree of crystallinity. For $Ni_{0.2}Co_{2.8}O_4$, the diffraction peaks found at 20.74°, 27.49°, 34.21°, 54.92°, 67.44° and 73.21° corresponds to (111), (220), (311), (440), (511) and (440), respectively. With the introduction of MWCNTs into $Ni_{0.2}Co_{2.8}O_4$, a dominant peak centered at 27.0° corresponds to the (002) which is attributed to carbonaceous phase related to the hexagonal graphite structures of MWCNTs, rest the peaks are indexed same as of $Ni_{0.2}Co_{2.8}O_4$ sample, this infers the successful incorporation of MWCNTs and $Ni_{0.2}Co_{2.8}O_4$. For $Ni_{0.2}Co_{2.8}O_4$/MWCNTs, a slight shift in (111) (with reference to pure $Ni_{0.2}Co_{2.8}O_4$) and the increase in the intensity of the diffraction peaks was observed. It inferred that the MWCNTs could intercalate between the layers or adsorb onto the surface of the oxide particles. This interaction may cause changes in the crystal structure, lattice parameters, or preferred orientations of the $Ni_{0.2}Co_{2.8}O_4$, leading to the shifting or disappearance of specific diffraction peaks associated with certain crystal planes. In $Ni_{0.2}Co_{2.8}O_4$/MWCNTs, we observed that with MWCNTs the diffraction peak intensity increased which inferred the well-organized dispersion of $Ni_{0.2}Co_{2.8}O_4$ within MWCNTs.

3.2. Morphological studies

Morphological analysis by SEM reflected uniform particle distribution and relatively smooth surface of $Ni_{0.2}Co_{2.8}O_4$, Fig. 2(a). While in case of $Ni_{0.2}Co_{2.8}O_4$/MWCNTs, Fig. 2(b), the surface seems rougher and porous confirming the high surface area which leads to improved super-capacitive performance. In Fig. 2(b)–a uniform and well dispersed deposition of $Ni_{0.2}Co_{2.8}O_4$ can be visualized on the surface of MWCNTs. The EDX spectra of both unsupported and supported materials are displayed in Fig. 2(c and d). The constituents Ni, and Co were well-coordinated in both synthesized samples. The presence of carbon was also envisioned in the supported sample which thoroughly confirms the formation of $Ni_{0.2}Co_{2.8}O_4$/MWCNTs.

3.3. Electrochemical investigations for supercapacitor

The synthesized materials were further investigated for their potency as anode candidates in supercapacitor and water splitting applications. The electrochemical investigation for supercapacitor was carried out by performing cyclic voltametric experiments at various scan rates (5, 10, 20, 50,100, 200, 500 mV/s). The redox activity of both materials is shown in Fig. 3 (a, b). The redox peaks at 0.36 V and 0.44 V, in $Ni_{0.2}Co_{2.8}O_4$ represented M–O/M–O–OH redox activity, where M denotes Ni or Co ions [36,37]. With the increase in scan rates the peak current increased for both materials ($Ni_{0.2}Co_{2.8}O_4$ and $Ni_{0.2}Co_{2.8}O_4$/MWCNTs) and the shift in redox peaks was noticed, which could be attributed to the transportation of ions towards electrode material.

The graphs were plotted between (Ip) *vs.* square root of scan rate, Fig. S1 in supplementary material), and diffusion co-efficient (D_o) was determined by the slope using Randles-Sevcik equation ($I_p = (2.99 \times 10^5)n[(1-\alpha)n_\alpha]^{1/2}AD_o^{1/2}Cv^{1/2}$). The D_o values were evaluated to be 1.08×10^{-2} cm^2s^{-1} and $1.56 \times 10^{-3}cm^2s^{-1}$, respectively, for $Ni_{0.2}Co_{2.8}O_4$ and $Ni_{0.2}Co_{2.8}O_4$/MWCNTs. The linear rise of current with scan rates further indicated the involvement of diffusion-controlled process and the lower D_o value for $Ni_{0.2}Co_{2.8}O_4$/MWCNTs authenticated slow diffusion due to massive material [38]. The relation between sp. capacitance and current is given as follows, [35].

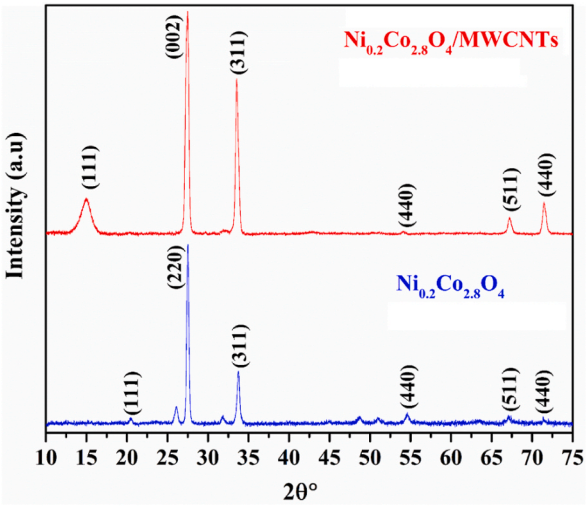

Fig. 1. Stacked XRD patterns of Ni0.2Co2.8O4 and Ni0.2Co2.8O4/MWCNTs.

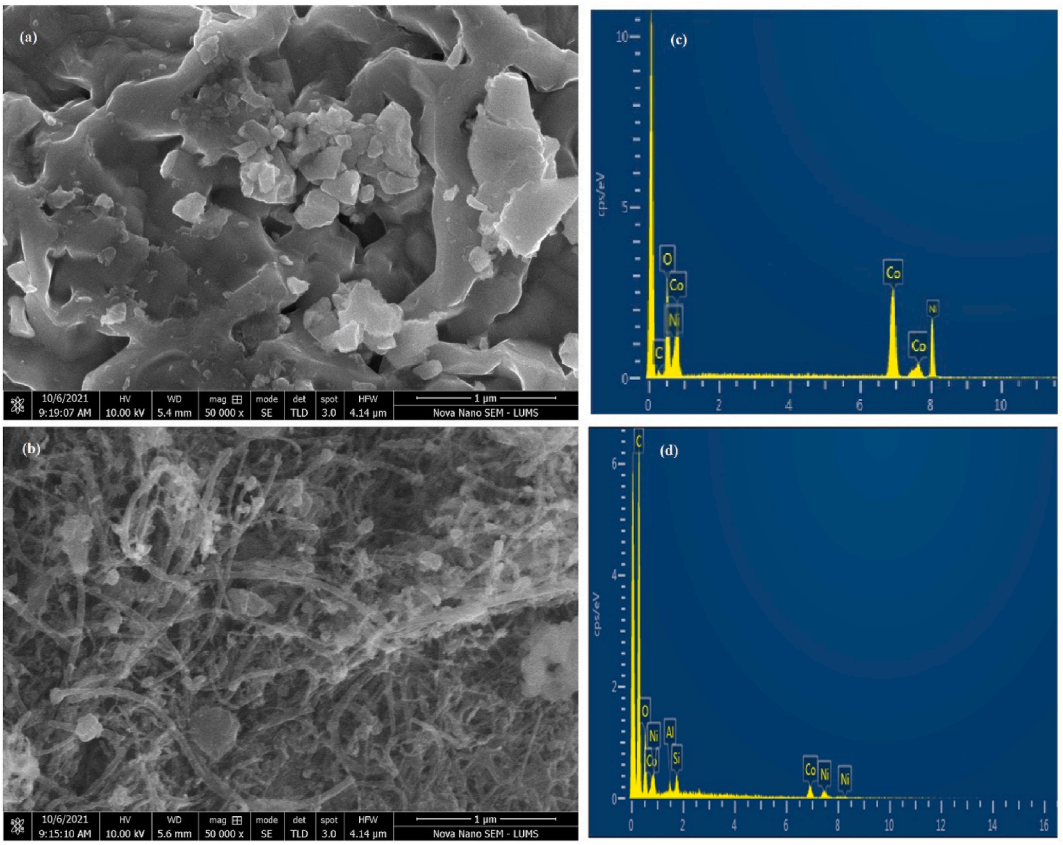

Fig. 2. SEM image of (a) $Ni_{0.2}Co_{2.8}O_4$ (b) $Ni_{0.2}Co_{2.8}O_4$/MWCNTs along with their (c, d) EDX spectra.

$$C_{SP} = \int Idv/2\ m\upsilon\Delta V \quad (1)$$

Where, ∫Idv shows the area under the curve, m, υ, and Δv, respectively, are electrode mass (1 mg), scan rate (Vs^{-1}), and potential range/window (0–0.7 V). The calculated C_{SP} values for $Ni_{0.2}Co_{2.8}O_4$ at 5 mV/s to 500 mV/s were evaluated to be 21.6, 10.8, 5.40, 2.16, 1.08, 0.54 and 0.216 Fg^{-1}, respectively, while for $Ni_{0.2}Co_{2.8}O_4$/MWCNTs these values were 505.8, 252.8, 126.3, 50.6, 25.3, 12.6, and 5.05 Fg^{-1} at same scan rate range (5–500 mV/s).

At the lowest scan rate of 5 mV/s, the C_{sp} value for $Ni_{0.2}Co_{2.8}O_4$/MWCNTs was evaluated to be ~23 times higher than the pristine $Ni_{0.2}Co_{2.8}O_4$ and inferred the excellent conductivity of the as-prepared $Ni_{0.2}Co_{2.8}O_4$/MWCNTs electrode. Further, the greater value of specific capacitance at slow scan rate may refers to interaction either due to penetration of ions into the pores of electrode or they diffused, while at higher scan rate, the interaction occurred only at surface of electrode [36]. The C_{sp} values, as evaluated greater for $Ni_{0.2}Co_{2.8}O_4$/MWCNTs than that for $Ni_{0.2}Co_{2.8}O_4$ at all scan rates, could be attributed to the fact that MWCNTs provided large active sites which ultimately enhanced the capacitance value of $Ni_{0.2}Co_{2.8}O_4$ [39]. Hence, the observed behavior inferred the comparatively more suitability of $Ni_{0.2}Co_{2.8}O_4$/MWCNTs for supercapacitor application. The scan rate effect on C_{sp} could be seen in Fig. 3(a, b; inset).

The $Ni_{0.2}Co_{2.8}O_4$/MWCNTs electrode maintained 85 % of the initial capacitance, which was higher than that of the pure $Ni_{0.2}Co_{2.8}O_4$ with 78 % capacitance retention at 1000 cycles, indicating relatively more cycling stability of hybrid electrode material. The higher cycling performance may be due to the synergetic effect of $Ni_{0.2}Co_{2.8}O_4$ with MWCNTs. This indicated that inclusion of MWCNTs played a crucial role in enhancing cycling life span of electrode material. The relation between capacitance retention and number of cycles is displayed in Fig. 3(c).

The galvanostatic charge/discharge profile of $Ni_{0.2}Co_{2.8}O_4$ and $Ni_{0.2}Co_{2.8}O_4$/MWCNTs was studied at different current densities of 0.5 A/g, 0.6 A/g and 0.7 A/g, Fig. 4 (a, b). At high current densities (0.6 and 0.7 A/g), $Ni_{0.2}Co_{2.8}O_4$ electrode suffered a sudden big potential drop (IR-drop) at the beginning of the discharge curve, while at comparatively low current density (0.5 A/g) the overall charging/discharging time was found to be around 650 s, Fig. 4 (a). The IR-drop is basically ascribed to the electrolyte's resistance and the ions' diffusion resistance which impacts on a capacitor in terms of its overall performance [40]. In case of $Ni_{0.2}Co_{2.8}O_4$/MWCNT, the entire charging/discharging time was found to be greater at all current densities with comparatively greater value (around 700 s) at low current density (0.5 A/g), Fig. 4 (b). The reviewed results revealed that the highest discharging time is mainly due to considerable surface area and inferred the suitability of the material for electrode in energy storage applications [41–43]. The C_{sp} values for both

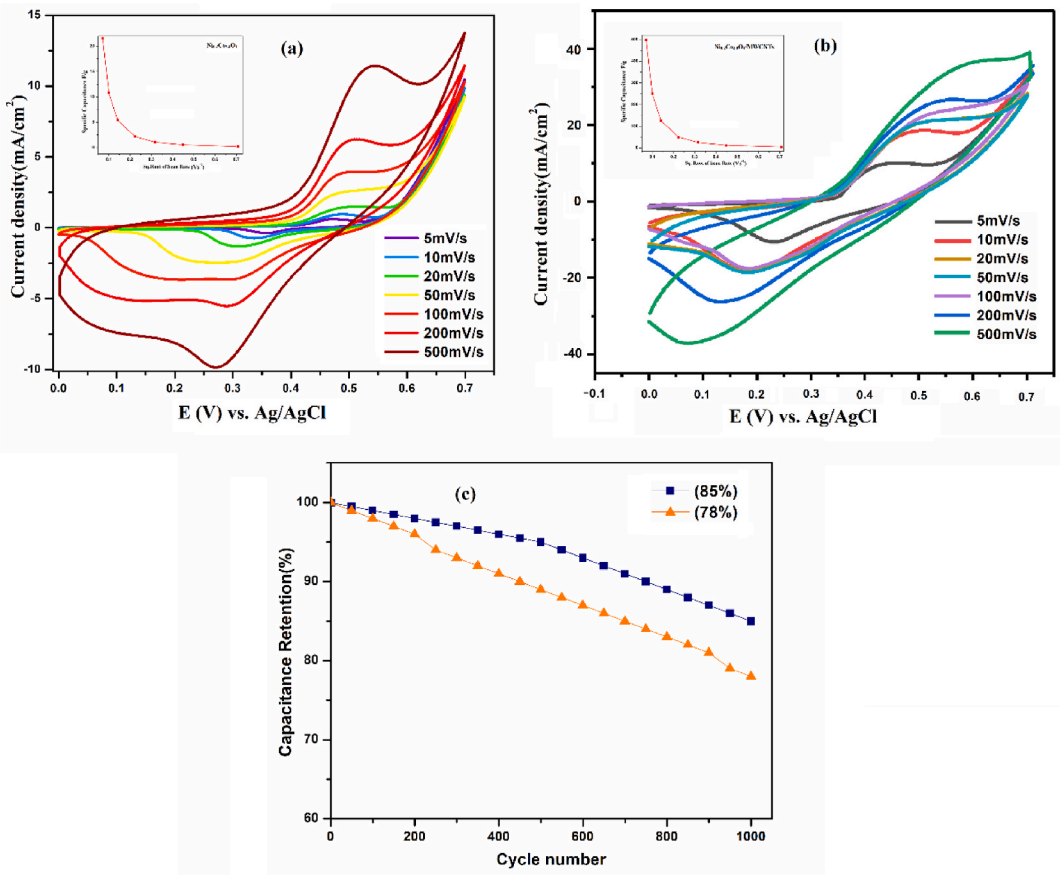

Fig. 3. Cyclic voltammograms of (a) $Ni_{0.2}Co_{2.8}O_4$ (b) $Ni_{0.2}Co_{2.8}O_4$/MWCNTs at scan rate range from 5 to 500 mV/s; Insets; plots representing changes in the C_{sp} with scan rate **(c)** Cyclic stability graphs.

materials were evaluated by using equation (2), [35,44].

$$C_{sp} = (Idt)/(m\Delta V) \tag{2}$$

Where I and dt, respectively, are charging/discharging current (A) discharging time (s), while other parameters (m, ΔV) are same as in Eq. (1). The specific capacitance (Fg^{-1}) values were calculated to be 57.3, 33.2 and 21.95 for $Ni_{0.2}Co_{2.8}O_4$ and 1598, 792 and 574 for $Ni_{0.2}Co_{2.8}O_4$/MWCNT at 0.5 A/g, 0.6 A/g and 0.7 A/g current density, respectively. The specific capacitance of both materials drastically decreased at 0.7 A/g that indicated kinetic hindrance due to potassium ion penetration at high current density [35,36].

The energy density (Ed) of each as-fabricated electrode was evaluated by using the values of specific capacitance (C_{SP}) in equation (3), while the power density (Pd) was obtained by using the value of Ed in equation (4), [35,44].

$$Ed = \frac{1}{2}\left(C_{SP} \times \Delta V^2\right)\ \frac{1}{3.6} \tag{3}$$

$$Pd = \frac{Ed}{dt}\ 3600 \tag{4}$$

In above equations, ΔV represents the potential window (0–0.7 V) and dt is the discharging time in seconds. The evaluated values of energy density and power density along with C_{sp} (Fg^{-1} from GCD) and dt (the time where materials discharged completely) are provided in Table S1 in supplementary material. The Ragone plots of $Ni_{0.2}Co_{2.8}O_4$ and $Ni_{0.2}Co_{2.8}O_4$/MWCNTs are displayed in Fig. 4 (c). In comparison to $Ni_{0.2}Co_{2.8}O_4$, $Ni_{0.2}Co_{2.8}O_4$/MWCNTs delivered a high energy density (Ed) of 109 Wh/kg at 1114 W/kg of power density (Pd) at 0.5 A/g and maintained at around 39.06 Wh/kg at 1559 W/kg at 0.7 A/g. The values indicated that supercapacitor efficiency of current hybrid is better than that of reported $NiCo_2O_4$@MWCNT for which these values were found less [36].

Fig. 5 displayed the overlay of Nyquist plot of $Ni_{0.2}Co_{2.8}O_4$ and $Ni_{0.2}Co_{2.8}O_4$/MWCNT along with the model of equivalent circuit that best fitted to measure EIS parameters, whereas individual Nyquist plots are provided as Fig. S2 in supplementary material. R_s, R_{ct}, CPE, and Z_w represented solution resistance, charge transfer resistance, constant phase element, and Warburg impedance, respectively. Since depressed semi-circles were featured in the Nyquist plots of both materials, the precise fitting was made by replacing the double

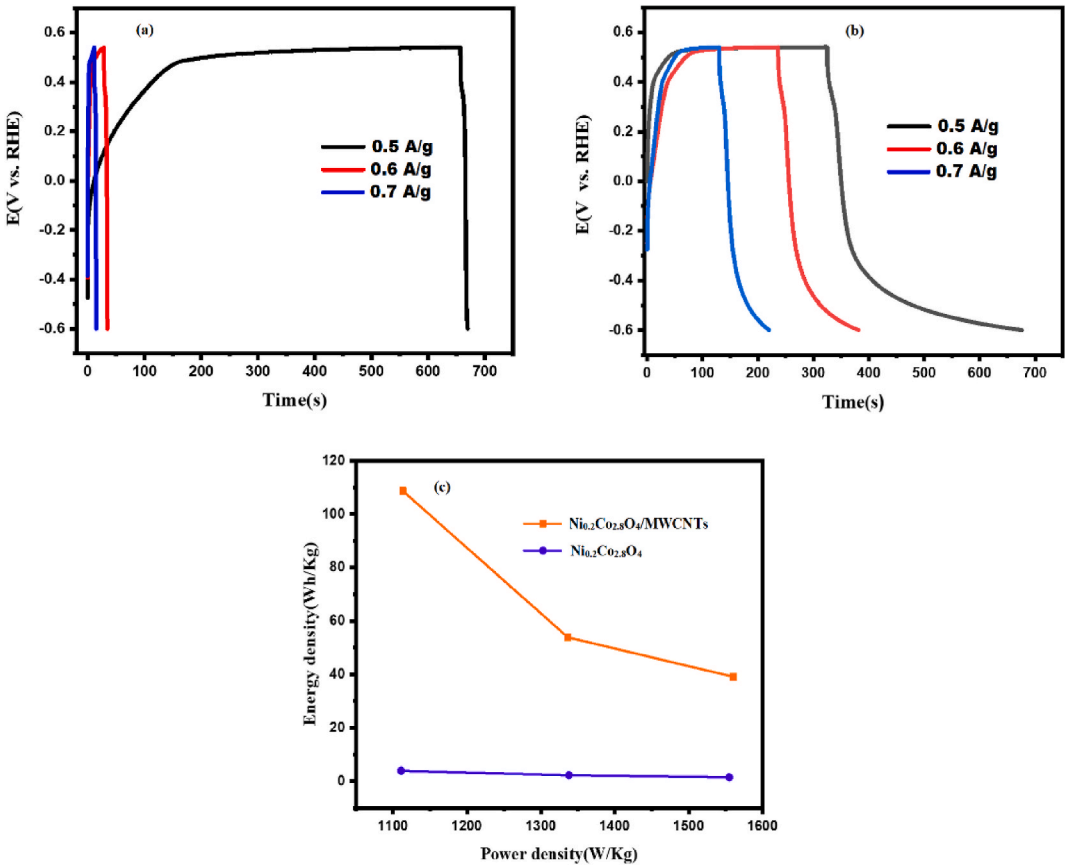

Fig. 4. GCD Graph of (a) $Ni_{0.2}Co_{2.8}O_4$ (b) $Ni_{0.2}Co_{2.8}O_4$/MWCNTs. **(c)** Ragone plots.

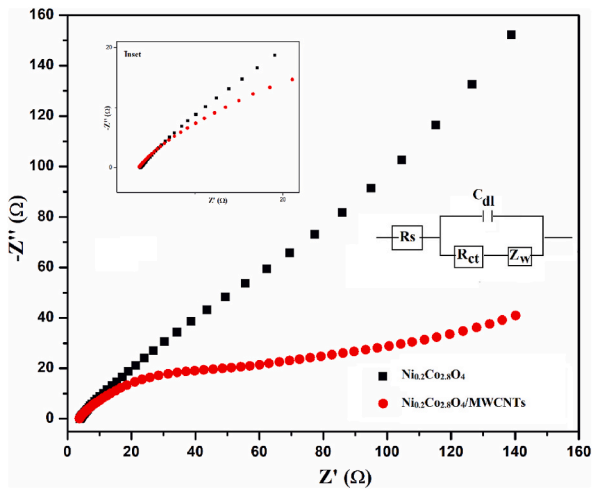

Fig. 5. Overlay Nyquist plot of $Ni_{0.2}Co_{2.8}O_4$ and $Ni_{0.2}Co_{2.8}O_4$/MWCNTs with model circuits topology. Inset: zoomed high frequency region representing stimulated circuit.

layer capacitance (C_{dl}) with CPE in the topology [45]. At the low frequency region, the linear portion of the response is related to Z_w and indicative of ions' diffusion onto the surface of electrode [35]. $Ni_{0.2}Co_{2.8}O_4$ showed high frequency semicircle on the real axis inferring solution resistance R_s (2.479 Ω) and low frequency tail resulted from the capacitance behavior of cobalt and nickel oxide, while for $Ni_{0.2}Co_{2.8}O_4$/MWCNTs, from the intercepts of the high-frequency semicircle on the real axis, the calculated solution resistance (R_s) was found to be 2.098 Ω. The calculated charge transfer resistance (R_{ct}) and capacitance (C_{dl}) values were found to be 4.21

Ω cm^2 and 12.64 F cm^2 for $Ni_{0.2}Co_{2.8}O_4$. However, for $Ni_{0.2}Co_{2.8}O_4$/MWCNTs, the diameter of arc within a high and middle frequency region gave lower R_{ct} (3.48 Ω cm^2) and higher C_{dl} (18.37 F cm^2) values which indicated a good contact between the electrode/electrolyte surfaces and could be inferred to have improved electrical conductivity of supported electrode material [35,46–48]. The comparatively lower R_{ct} of $Ni_{0.2}Co_{2.8}O_4$/MWCNTs could be attributed to the formation of new interfaces in a composite that may facilitate electrons transfer hence resulted in lower charge transfer resistance.

3.4. Electrochemical investigations for OER in water splitting

LSV was performed parallel to CV to support the results obtained from CV. The onset and over potential values, as taken from both CV and LSV, were found almost similar. The CV and LSV voltammograms for $Ni_{0.2}Co_{2.8}O_4$ and $Ni_{0.2}Co_{2.8}O_4$/MWCNTs with compensated IR-drop are shown in Fig. 6 (a, b), while with uncompensated IR-drop, provided as Fig. S3 in supplementary material. The onset potential was found to be 1.55 V (vs. RHE) while the over potential was evaluated to be 380 mV at current density of 100 mA/cm^2 for $Ni_{0.2}Co_{2.8}O_4$. In the case of supported material $Ni_{0.2}Co_{2.8}O_4$/MWCNTs, the onset potential was not clear as the oxidation peak is present in this region, while the over potential was found to be 340 mV @100 mA/cm^2. These values validated the reliability of both investigated materials for OER performance. Overall, the lower over potential for $Ni_{0.2}Co_{2.8}O_4$/MWCNTs pointed out this material to have comparatively better anode candidacy for OER in water splitting process.

The Tafel slopes, as obtained from LSV, are shown in Fig. 7 (a). $Ni_{0.2}Co_{2.8}O_4$ /MWCNTs showed low Tafel slope value of 47 mV/dec as compared to $Ni_{0.2}Co_{2.8}O_4$ which was found to be 71 mV/dec. The lower Tafel slope for $Ni_{0.2}Co_{2.8}O_4$/MWCNTs revealed minimum potential changes per decade; hence could be attributed to its comparatively more suitability as an electrocatalyst for long lasting water splitting [35,49,50].

Further, the stability of synthesized materials was checked by chronoamperometric protocol and current density vs. time graphs were plotted, Fig. 7(b). The controlled potential electrolysis (CPE) revealed that at current density of 19 $mAcm^{-2}$ and 23 mA/cm^2 for $Ni_{0.2}Co_{2.8}O_4$ and $Ni_{0.2}Co_{2.8}O_4$/MWCNTs, respectively, these materials remained stable at selected span of time for OER in water oxidation [51,52].

Overall, the better performance of supported material for both supercapacitor and OER water splitting applications could be associated with large surface area and high conductivity of MWCNTs.

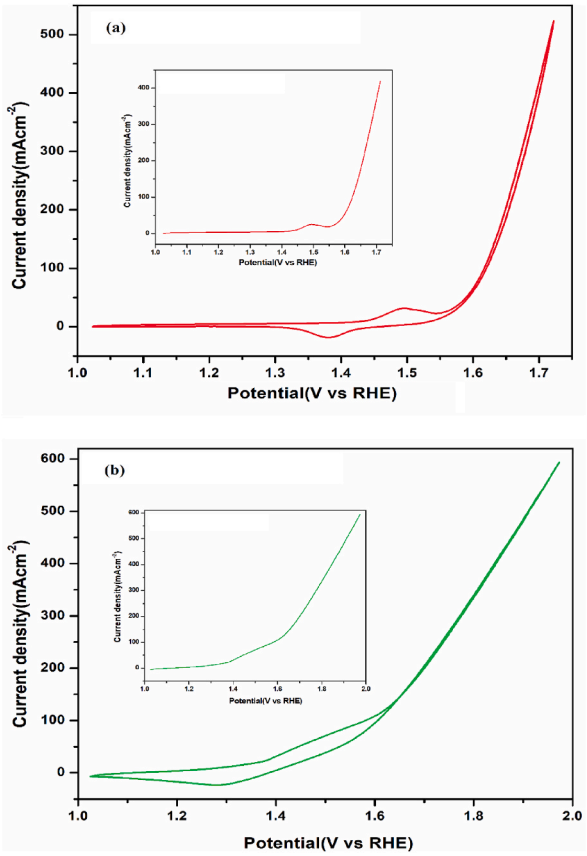

Fig. 6. CV and LSV (inset) voltammograms of (a) $Ni_{0.2}Co_{2.8}O_4$ and (b) $Ni_{0.2}Co_{2.8}O_4$/MWCNTs with compensated IR-drop.

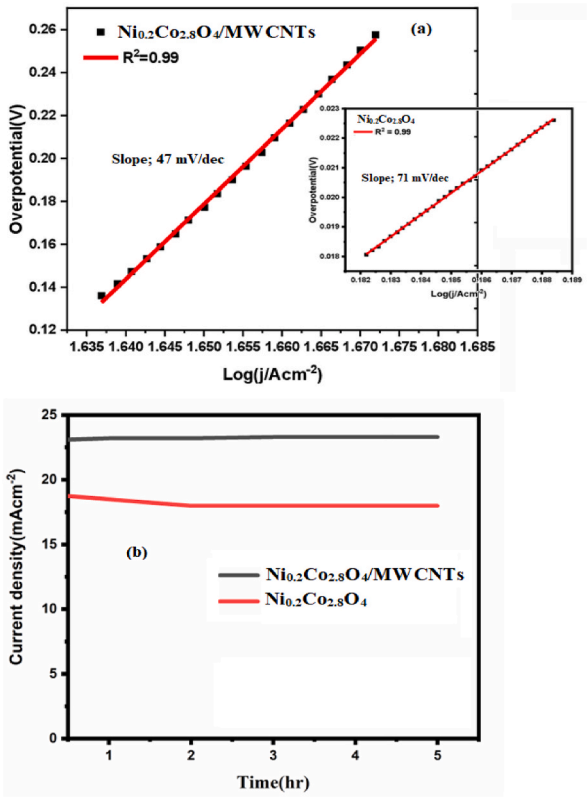

Fig. 7. Tafel slopes of (a) $Ni_{0.2}Co_{2.8}O_4$/MWCNTs, (inset; $Ni_{0.2}Co_{2.8}O_4$) (b) CPE graphs.

3.5. Electrochemical performance comparative studies

Herein, Table 1 is provided to compare our elucidated electrochemical parameters for supercapacitor and OER with that reported for Ni–Co based electrocatalysts. It could be seen from Table 1 that the capacitance value at low scan rate for the $Ni_{0.2}Co_{2.8}O_4$/MWCNTS, in current study, is well improved and high as compared to reported $NiCo_2O_4$ and its composites with carbon nano tubes [35,36,53]. Also, parameters in Table 1 indicate better OER performance of studied materials in comparison to some benchmark NiCo based electrocatalysts [53–58]. The overpotential values of studied electrocatalysts for OER were evaluated @100mAcm^{-2} and found comparative and even lower than that evaluated for reported Ni–Co based electrocatalysts @10mAcm^{-2}. Table 1 also provides a comparison with bare Ni-foam for supercapacitor and OER parameters [59,60]. These comparisons further supported our findings for the studied materials, particularly for $Ni_{0.2}Co_{2.8}O_4$/MWCNTs to have efficient and sustainable anode candidacy to be used in both supercapacitor and OER applications.

4. Conclusions

The anode candidacy of $Ni_{0.2}Co_{2.8}O_4$ and $Ni_{0.2}Co_{2.8}O_4$/MWCNTs for supercapacitor and OER water splitting applications was monitored via electrochemical performance studies. Among the two, the supported catalyst $Ni_{0.2}Co_{2.8}O_4$/MWCNTs achieved high specific capacitance of 505.8 Fg^{-1} at 5 mV/s (CV) and 1598 Fg^{-1} at 0.5 A/g (GCD). The same material showed a high discharging rate at low current density (0.5 A/g), lower charge transfer resistance (R_{ct}; 3.48 Ω cm^2), and high capacitance retention (85 %) of after 1000 cycles. These findings made the integrated material ($Ni_{0.2}Co_{2.8}O_4$/MWCNTs) advantageous over $Ni_{0.2}Co_{2.8}O_4$ for super-capacitor applications. The OER results for water splitting also revealed the supported material ($Ni_{0.2}Co_{2.8}O_4$/MWCNTs) an efficient electro-catalyst in terms of comparatively lower over potential, Tafel slope, and indelible stability at current density of 23 mAcm^{-2} in 1.0 M KOH. Conclusively, our findings could propose $Ni_{0.2}Co_{2.8}O_4$/MWCNTs a potential anode candidate to be used as electrocatalyst for supercapacitor and OER water splitting applications.

Funding

This research has been supported by Researchers Supporting Project number (RSPD2024R979), King Saud University, Riyadh, Saudi Arabia.

Table 1
Comparison of the electrochemical parameters for supercapacitor and OER applications in alkaline media.

Anode material	Substrate	Supercapacitor parameters				OER parameters			Reference
		C_{sp} (Fg^{-1})	Energy density (Whkg-1)	Power density (Wkg-1)	$Rs(\Omega)/R_{ct}$ (Ωcm^2)/C_{dl} (Fcm^2)	Onset potential (V) (vs RHE)	Over Potential (mV)	Tafel slope $mVdec^{-1}$	
$Ni_{0.2}Co_{2.8}O_4$	Ni-foam	CV:21.6 @ 5 mVs^{-1} GCD:57.3(@ 0.5Ag^{-1}	3.99@ 0.5 Ag^{-1}	1113@ 0.5 Ag^{-1}	2.479/4.21/ 12.64	1.55	380	71	Current work
$Ni_{0.2}Co_{2.8}O_4$/ MWCNTs	Ni-foam	CV: 505.8 @ 5 mVs^{-1} GCD:1598@ 0.5Ag^{-1}	109@ 0.5 Ag^{-1}	1114@ 0.5 Ag^{-1}	2.098/3.48/ 18.37	–	340	47	Current work
NCO@MWCNT	Ni-foam	CV:114@ 10 mVs^{-1}) GCD: 374@ 2 Ag^{-1}	95@ 2 Ag^{-1}	3964@ 2 Ag^{-1}	./2.857/.	–	–	–	[36]
$NiCo_2O_4$ nanograss	CNT/SS	GCD:1223@ 1 Ag^{-1}	34.4	225	1.46/0.04/.	–	–	–	[37]
Co_3O_4/$NiCo_2O_4$ DSNs	Ni-foam	972@5 Ag^{-1}	–	–	–	1.53	340	88	[53]
$Ni_xCo_yMn_zO_4$ calcinated at 300 °C	GC-electrode	–	–	–	5.0/./.	1.7	400	74	[54]
NiCo nano-needles	CNTs/CF	–	–	–	./~20/.	1.62	320	82	[55]
$NiCo_2O_4$, $NiCo_2O_4$/GNs	GC -electrode	–	–	–	–	1.53, 1.50	428, 383	141, 137	[56]
$NiCo_2O_4$	FTO@400 °C	–	–	–	–	1.55	375	54	[57]
NiCo-LDH-NA	CF-paper	–	–	–	–	–	307	64	[58]
Bare Ni-foam	Nickel foam	35@10 mVs^{-1}	–	–	5.87/./.	1.556	337	97	[59] [60]

Data availability statement

Data will be made available on request.

CRediT authorship contribution statement

Sana Sabahat: Writing - review & editing, Writing - original draft, Validation, Supervision, Project administration, Methodology, Conceptualization. **Nasima Arshad:** Writing - review & editing, Writing - original draft, Validation, Supervision, Project administration, Methodology, Conceptualization. **Nida Aftab:** Software, Investigation, Formal analysis, Data curation. **Zeeshan Mujtaba:** Software, Methodology, Formal analysis, Data curation. **Mohd Afzal:** Writing - review & editing, Funding acquisition, Formal analysis. **Maria Christy:** Formal analysis.

Declaration of competing interest

The authors declare that they have no known competing financial interests or personal relationships that could have appeared to influence the work reported in this paper.

Acknowledgments

The authors would like to thank all departments of mentioned universities for research facilities. Dr. Mohd Afzal extends his appreciation to Researchers Supporting Project number (RSPD2024R979), King Saud University, Riyadh, Saudi Arabia.

Appendix B. Supplementary data

Supplementary data to this article can be found online at https://doi.org/10.1016/j.heliyon.2024.e24214.

References

[1] N. S Rathore, N. Panwar, Renewable Energy Sources for Sustainable Development, first ed., New Indian Publishing Agency, 2007. ISBN 10: 8189422723/ISBN 13: 9788189422721.
[2] M.B. Arvas, M. Gencten, Y. Sahin, One-step synthesized N-doped graphene-based electrode materials for supercapacitor applications, Ionics 27 (2021) 2241–2256.
[3] M.B. Arvas, M. Gencten, Y. Sahin, Supercapacitor applications of novel phosphorus doped graphene-based electrodes, J. Energy Storage 55 (2022) 105766.
[4] Y. Zhang, C. gang Zhou, X.- hua Yan, Y. Cao, H.- li Gao, H.- wei Luo, K. zheng Gao, S. chang Xue, X. Jing, Recent advances and perspectives on graphene-based gels for superior flexible all-solid-state supercapacitors, J. Power Sources 565 (1) (2023) 232916.
[5] Y. Zhang, H. xin Mei, Y. Cao, X. hua Yan, J. Yan, H. li Gao, H. wei Luo, S. wen Wang, X. dong Jia, L. Kachalova, J. Yang, S. chang Xue, C. gang Zhou, L. xia Wang, Y. hai Gui, Recent advances and challenges of electrode materials for flexible supercapacitors, Coord. Chem. Rev. 438 (1) (2021), 213910 1-21391030.
[6] M.B. Arvas, N. Karatepe, M. Gencten, Y. Sahin, One-step synthesis of nitrogen-doped graphene powders and application of them as high-performance symmetrical coin cell supercapacitors in different aqueous electrolyte, Int. J. Energy Res. 46 (6) (2022) 7348–7373.
[7] M.B. Arvas, N. Karatepe, M. Gencten, Y. Sahin, Fabrication of S,N co-doped graphene powders for symmetrical supercapacitors in different aqueous electrolytes, J. Mater. Sci. Mater. Electron. 34 (12) (2023) 1068.
[8] D. Chen, Q. Wang, R. Wang, G. Shen, Ternary oxide nanostructured materials for supercapacitors: a review, J. Mater. Chem. A 31 (9) (2015) 10158–10173.
[9] X. Dong, X. Jing, Y. Mu, Y. Yu, C. Miao, C. Meng, C. Huang, Y. Zhang, Rational design of double-sandwich-like C@ Co, CoO/Co_2SiO_4/rGO architectures boost electrochemical performances of Co_2SiO_4 for energy storage devices, Chem. Eng. J. 431 (2022) 133277.
[10] Y. Zhang, C. Wang, X. Chen, X. Dong, C. Meng, C. Huang, Bamboo leaves as sustainable sources for the preparation of amorphous carbon/iron silicate anode and nickel–cobalt silicate cathode materials for hybrid Supercapacitors, ACS Appl. Energy Mater. 4 (9) (2021) 9328–9340.
[11] Y. Zhang, S. chang Xue, X.- hua Yan, H.- li Gao, X. Jing, K. zheng Gao, Y. Cao, H.- wei Luo, J. Yan, Synthesis of CoAl-LDH@Ni(OH)2 high-performance supercapacitor electrode composites by hydrothermal-assisted electrodeposition, Ionics 28 (11) (2022) 5211–5222.
[12] Y. Zhang, S. chang Xue, X.- hua Yan, H.- Li Gao, K. zheng Gao, Preparation and electrochemical properties of cobalt aluminum layered double hydroxide/carbon-based integrated composite electrode materials for supercapacitors, Electrochim. Acta 442 (2023) 141822.
[13] Y. Zhang, H.- xin Mei, J. Yang, H.- Li Gao, X.- Dong Jia, Facile synthesis of novel parallelogram-like $NH_4CoPO_4{\cdot}H_2O$/$Ni_3(PO_4)_2{\cdot}8H_2O$/MnO_2 composites for high-performance supercapacitors, J. Electrochem. Energy Convers. Storage 18 (1) (2020) 1–20.
[14] W.H. Low, P.S. Khiew, S.S. Lim, C.W. Siong, E.R. Ezeigwe, Recent development of mixed transition metal oxide and graphene/mixed transition metal oxide based hybrid nanostructures for advanced supercapacitors, J. Alloys Compd. 775 (2019) 1324–1356.
[15] Z. Wu, Y. Zhu, X. Ji, NiCo2O4-based materials for electrochemical supercapacitors, J. Mater. Chem. A 2 (36) (2014) 14759–14772.
[16] D.P. Dubal, P. Gomez-Romero, B.R. Sankapal, R. Holze, Nickel cobaltite as an emerging material for supercapacitors: an overview, Nano Energy 11 (2015) 377–399.
[17] S. Iijima, Synthesis of carbon nanotubes, Nature 354 (1991) 56–58.
[18] Q. Zhang, M. Zhu, Q. Zhang, Y. Li, H. Wang, The formation of magnetite nanoparticles on the sidewalls of multi-walled carbon nanotubes, Compos. Sci. Technol. 69 (5) (2009) 633–638.
[19] V. Gupta, T.A. Saleh, in: S. Bianco (Ed.), Syntheses of Carbon Nanotube-Metal Oxides Composites; Adsorption and Photo-Degradation, Carbon Nanotubes - from Research to Applications, InTechOpen, 2011. ISBN: 978-953-307-500-6.
[20] K. Sun, Z. Zhang, B. Gao, Z. Wang, D. Xu, J. Jin, X. Liu, Adsorption of diuron, fluridone and norflurazon on single-walled and multi-walled carbon nanotubes, Sci. Total Environ. 439 (2012) 1–7.
[21] N. Li, J. Chen, Y.P. Shi, Magnetic graphene solid-phase extraction for the determination of carbamate pesticides in tomatoes coupled with high performance liquid chromatography, Talanta 141 (2015) 212–219.
[22] J. Dong, Z. Feng, S. Kang, M. An, G. Wu, Magnetic solid-phase extraction based on magnetic amino modified multiwalled carbon nanotubes for the fast determination of seven pesticide residues in water samples, Anal. Methods 12 (21) (2020) 2747–2756.
[23] M. Alghuthaymi, A. Amal, M. Mostafa, K.A. Abd-Elsalam, Carbon Nanomaterials for Agri-Food and Environmental Applications, Elsevier, Amsterdam, The Netherlands, 2020, pp. 429–457.
[24] A. Stegarescu, H. Cabrera, H. Budasheva, M.L. Soran, I. Lung, F. Limosani, D. Korte, M. Amati, G. Borodi, I. Kacso, O. Opriş, Synthesis and characterization of MWCNT-COOH/Fe_3O_4 and CNT-COOH/Fe_3O_4/NiO nanocomposites: assessment of adsorption and photocatalytic performance, Nanomaterials 12 (17) (2022) 3008.
[25] S. Al-Rubaye, R. Rajagopalan, S.X. Dou, Z. Cheng, Facile synthesis of a reduced graphene oxide wrapped porous $NiCo_2O_4$ composite with superior performance as an electrode material for supercapacitors, J. Mater. Chem. A 5 (36) (2017) 18989–18997.
[26] L. Ma, X. Shen, H. Zhou, Z. Ji, K. Chen, G. Zhu, High performance supercapacitor electrode materials based on porous $NiCo_2O_4$ hexagonal nanoplates/reduced graphene oxide composites, Chem. Eng. J. 262 (2015) 980–988.
[27] Z. Yang, J. Tian, Z. Yin, C. Cui, W. Qian, F. Wei, Carbon nanotube-and graphene-based nanomaterials and applications in high-voltage supercapacitor: a review, Carbon 141 (2019) 467–480.
[28] A. Akanksha, M. Sutripto, S.R. Babasaheb, Carbon nanotube-functionalized surface-assisted growth of cobalt phosphate nanodots: a highly stable and bendable all-solid-state symmetric supercapacitor, Energy Fuels 36 (11) (2022) 5953–5964.
[29] A. Akanksha, M. Sutripto, S.R. Babasaheb, Multi-walled carbon nanotubes supported copper phosphate microflowers for flexible solid-state supercapacitor, Int. J. Energy Res. 46 (5) (2021) 6177–6196.
[30] A. Akanksha, M. Sutripto, S.R. Babasaheb, Ni3P2O8 nanodots anchored multiwalled carbon nanotubes composite for flexible all-solid-state symmetric supercapacitor, J. Energy Storage 58 (2023) 106396.
[31] H. Zhang, H. Guo, X. Deng, P. Gu, Z. Chen, Z. Jiao, Functionalization of multi-walled carbon nanotubes via surface unpaired electrons, Nanotechnology 21 (8) (2010) 085706.
[32] P. Azadi, R. Farnood, E. Meier, Preparation of multiwalled carbon nanotube-supported nickel catalysts using incipient wetness method, J. Phys. Chem. A 114 (11) (2010) 3962–3968.
[33] J.A. Schwarz, C. Contescu, A. Contescu, Methods for preparation of catalytic materials, Chem. Rev. 95 (3) (1995) 477–510.
[34] S.D. Mhlanga, K.C. Mondal, R. Carter, M.J. Witcomb, N.J. Coville, The effect of synthesis parameters on the catalytic synthesis of multiwalled carbon nanotubes using Fe-Co/$CaCO_3$ catalysts, S. Afr. J. Chem. 62 (2009) 67–76.
[35] Z. Mujtaba, N. Arshad, Moringa oleifera and its spent tea waste composites as sustainable anode candidates for energy storage applications: Morphological and electrochemical performance studies, Mater. Chem. Phys. 301 (2023) 127576.
[36] M. Pathak, J.R. Jose, B. Chakraborty, C.S. Rout, High performance supercapacitor electrodes based on spinel $NiCo_2O_4$@ MWCNT composite with insights from density functional theory simulations, J. Chem. Phys. 152 (2020) 064706.
[37] M.S. Wu, Z.B. Zheng, Y.S. Lai, J. J Jow, Nickel cobaltite nanograss grown around porous carbon nanotube-wrapped stainless steel wire mesh as a flexible electrode for high-performance supercapacitor application, Electrochim. Acta 182 (2015) 31–38.
[38] K. Thiagarajan, D. Balaji, J. Madhavan, J. Theerthagiri, S.J. Lee, K.Y. Kwon, M.Y. Choi, Cost-effective synthesis of efficient $CoWO_4$/Ni nanocomposite electrode material for supercapacitor applications, Nanomaterials 10 (11) (2020) 2195.
[39] C. Nolly, C.O. Ikpo, M.M. Ndipingwi, P. Ekwere, E.I. Iwuoha, Pseudocapacitive effects of multi-walled carbon nanotubes-functionalised spinel copper manganese oxide, Nanomaterials 12 (2022) 3514.
[40] C. Wu, X. Wang, B. Ju, L. Jiang, H. Wu, Q. Zhao, L. Yi, Supercapacitive performance of nitrogen-enriched carbons from carbonization of polyaniline/activated mesocarbon microbeads, J. Power Sources 227 (2013) 1–7.

[41] X. Wang, X. Han, M. Lim, N. Singh, C.L. Gan, M. Jan, P.S. Lee, Nickel cobalt oxide-single wall carbon nanotube composite material for superior cycling stability and high-performance supercapacitor application, J. Phys. Chem. C 116 (23) (2012) 12448–12454.
[42] D. Zhang, H. Yan, Y. Lu, K. Qiu, C. Wang, Y. Zhang, X. Liu, J. Luo, Y. Luo, $NiCo_2O_4$ nanostructure materials: morphology control and electrochemical energy storage, Dalton Trans. 43 (42) (2014) 15887–15897.
[43] H. Chen, J. Jiang, L. Zhang, T. Qi, D. Xia, H. Wan, Facilely synthesized porous $NiCo_2O_4$ flowerlike nanostructure for high-rate supercapacitors, J. Power Sources 248 (2014) 28–36.
[44] O. Aydin, B. Birol, M. Gencten, Production of ZnS based supercapacitor electrode material from ferrochrome ash waste, Ionics 29 (2023) 3335–3352.
[45] N. Arshad, M. Akram, F. Altaf, A. Yaqub, Anti-corrosive potentials of 1, 2, 4-Triazole-5-thiones for mild steel 1030 in acidic environment, Protect. Met. Phys. Chem. Surface 56 (2020) 816–825.
[46] Y. Xie, H. Du, Electrochemical capacitance of a carbon quantum dots–polypyrrole/titania nanotube hybrid, RSC Adv. 5 (109) (2015) 89689–89697.
[47] T. Basili, H.Y. Kalyon, M. Gencten, M. Macita, Y. Sahin, High performance supercapacitive behaviors of oximes in a poly(aniline-co-pyrrole) based conducting polymer structure, New J. Chem. 47 (2023) 691–707.
[48] S. Yasa, B. Birol, M. Gencten, Recovery of cobalt as CoS from spent Li-ion batteries and investigation of its use as an electrode material for supercapacitors, New J. Chem. 47 (2023) 6224–6234.
[49] Y.H. Fang, Z.P. Liu, Tafel kinetics of electrocatalytic reactions: from experiment to first-principles, ACS Catal. 4 (12) (2014) 4364–4376.
[50] C. Mahala, M. Basu, Nanosheets of $NiCo_2O_4$/NiO as efficient and stable electrocatalyst for oxygen evolution reaction, ACS Omega 2 (11) (2017) 7559–7567.
[51] J. Theerthagiri, A.P. Murthy, S.J. Lee, K. Karuppasamy, S.R. Arumugam, Y. Yu, M.M. Hanafiah, H.S. Kim, V. Mittal, M.Y. Choi, Recent progress on synthetic strategies and applications of transition metal phosphides in energy storage and conversion, Ceram. Int. 47 (4) (2021) 4404–4425.
[52] C.A. Ottoni, C.D. Ramos, R.F.B. De Souza, S.G. Da Silva, E.V. Spinace, A.O. Neto, Glycerol and ethanol oxidation in alkaline medium using PtCu/C electrocatalysts, Int. J. Electrochem. Sci. 13 (2) (2018) 1893–1904.
[53] H. Hu, B. Guan, B. Xia, X.W. Lou, Designed formation of Co_3O_4/$NiCo_2O_4$ double-shelled nanocages with enhanced pseudocapacitive and electrocatalytic properties, J. Am. Chem. Soc. 137 (2015) 5590–5595.
[54] T. Priamushko, R. Guillet-Nicolas, M. Yu, M. Doyle, C. Weidenthaler, H. Tüysüz, F. Kleitz, Nanocast mixed Ni–Co–Mn oxides with controlled surface and pore structure for electrochemical oxygen evolution reaction, ACS Appl. Energy Mater. 3 (6) (2020) 5597–5609.
[55] T.N. Pham, A. Samikannu, S. Tesfalidet, T. Wågberg, J.P. Mikkola, NiCo nanoneedles on 3D carbon nanotubes/carbon foam electrode as an efficient Bi-functional catalyst for electro-oxidation of water and methanol, Catalysts 11 (4) (2021) 500.
[56] Z. Li, B. Li, J. Chen, Q. Pang, P. Shen, Spinel $NiCo_2O_4$ 3-D nanoflowers supported on graphene nanosheets as efficient electrocatalyst for oxygen evolution reaction, Int. J. Hydrogen Energy 44 (31) (2019) 16120–16131.
[57] J. He, Y. Sun, M. Wang, Z. Geng, X. Wu, L. Wang, H. Chen, K. Huang, S. Feng, Direct growth of $NiCo_2O_4$ nanostructure on conductive substrate by electrospray technique for oxygen evolution reaction, J. Alloys Compd. 752 (2018) 389–394.
[58] C. Yu, Z. Liu, X. Han, H. Huang, C. Zhao, J. Yang, J. Qiu, NiCo-layered double hydroxides vertically assembled on carbon fiber papers as binder-free high-active electrocatalysts for water oxidation, Carbon 110 (2016) 1–7.
[59] N.A. Salleh, S. Kheawhom, A.A. Mohamad, Characterizations of nickel mesh and nickel foam current collectors for supercapacitor application, Arab. J. Chem. 13 (8) (2020) 6838–6846.
[60] X. Hu, X. Tian, Y.W. Lin, Z. Wang, Nickel foam and stainless steel mesh as electrocatalysts for hydrogen evolution reaction, oxygen evolution reaction and overall water splitting in alkaline media, RSC Adv. 9 (54) (2019) 31563–31571.